IEEE Access
Multidisciplinary | Rapid Review | Open Access Journal

Received October 5, 2020, accepted October 26, 2020, date of publication November 3, 2020, date of current version November 12, 2020.

Digital Object Identifier 10.1109/ACCESS.2020.3035510

SMA-Driven Soft Robotic Neck: Design, Control and Validation

DORIN COPACI, JORGE MUÑOZ, (Member, IEEE), IGNACIO GONZÁLEZ, CONCEPCIÓN A. MONJE, (Member, IEEE), AND LUIS MORENO, (Member, IEEE)
Department of Systems Engineering and Automation, Carlos III University of Madrid, 28911 Leganés, Spain

Corresponding author: Dorin Copaci (dcopaci@ing.uc3m.es)

This work was supported in part by the Spanish Ministry of Economy and Competitiveness through the Exoesqueleto para Diagnostico y Asistencia en Tareas de Manipulación Spanish Research Project under Grant DPI2016-75346-R and the HUMASOFT Project under Grant DPI2016-75330-P, in part by the Programas de Actividades I+D en la Comunidad de Madrid through the RoboCity2030-DIH-CM Madrid Robotics Digital Innovation Hub (Robótica aplicada a la mejora de la calidad de vida de los ciudadanos, fase IV) under Grant S2018/NMT-4331, and in part by the Structural Funds of the EU.

ABSTRACT Replicating the behavior and movement of living organisms to develop robots which are better adapted to the human natural environment is a major area of interest today. Soft device development is one of the most promising and innovative technological fields to meet this challenge. However, soft technology lacks of suitable actuators, and therefore, development and integration of soft actuators is a priority. This article presents the development and control of a soft robotic neck which is actuated by a flexible Shape Memory Alloy (SMA)-based actuator. The proposed neck has two degrees of freedom that allow movements of inclination and orientation, thus approaching the actual movement of the human neck. The platform we have developed may be considered a real soft robotic device since, due to its flexible SMA-based actuator, it has much fewer rigid parts compared to similar platforms. Weight and motion noise have also been considerably reduced due to the lack of gear boxes, housing and bearings, which are commonly used in conventional actuators to reduce velocity and increase torque.

INDEX TERMS Bio-inspired neck, soft robotics, SMA actuators, motion-noise reduction.

I. INTRODUCTION

Soft robotic applications offer certain advantages compared to robots with rigid elements: they are more adaptable and accessible to complex environments, they present under-actuated architectures, and they are safer when they interact with the environment. On the other hand, soft robotic applications are more difficult to develop due to the current limitations of actuation systems (most actuators have a rigid structure) and are more difficult to control. One of the fields of interest in robotics applications is the development of bio-inspired systems that can simulate human movements. The biomechanics of human body is represented by a complex structure where different segments, soft tissues and ligaments, actuated by a coordinated group of muscles, determine movement. Human joints do not act as a single axis joint and most of them have different degrees of freedom (DOF) such as rolling, sliding or a combination of both, as in the elbow joint, for example [1]. Bio-inspired robotics tries to develop soft and flexible robots that can be easily adapted to the human environment, including the most complex movements, which are typically those of shoulder, hand or spine joints.

In the last decade, multiple humanoid neck structures have been proposed that can be classified into two categories: serial configuration – where each DOF is independently actuated – and parallel configuration – which consists of a mobile base, a fixed base, a backbone that connects the mobile base to the fixed base, and several tendons –, usually independently actuated [2]. The first category of neck is a rigid structure with 2, 3 or 4 joints, each with 1 DOF. Some examples of those configurations on humanoids robots are: with 2 DOF (Yaw and Pitch movement of the head), ASIMO humanoid [3], HUBO [4], HRP-4 [5], NAO [6], TORO [7], Pepper [8], Marko [9], Woody [10], a humanoid with a wheeled mobile base [11]; with 3 DOF (movements on the yaw, roll and pitch axes), Albert HUBO [12], HRP-4C [13], iCub [14]; with 4 DOF (movements of yaw, roll and upper and lower pitch), ROMAN [15], SAYA [16], Romeo [17]. The second

The associate editor coordinating the review of this manuscript and approving it for publication was Nishant Unnikrishnan.

category has a large number of DOF due to the backbone, which is usually composed by 3-7 vertebrae. The elastic and soft elements of this type of neck allow the head to have more natural, although less accurate, movements, compared to the first neck category. This second category with yaw, roll and pitch movements, are included in humanoids: Kenta [18], Kenshiro [19], Kengoro [20], Kotaro [21], LARMbot [22]. This category also includes a flexible humanoid spine structure [23], [24], [25], usually based on tendon driven or muscle-skeletal systems of actuation. Most of these applications use a DC motor actuation system, which increases the weight of the final device. Also, due to the motor gears, they have noisy operation, which is a limitation for systems that aim to mimic human behavior.

In recent years, the presence of smart materials has grown in various engineering areas, and they have been used to create actuators or just pieces of smart structures. The characteristics of these materials make them a good solution, especially when conventional motors have certain limitations. Shape Memory Alloy (SMA) is a special contributor. This type of material has a shape memory effect (SME), a transformation phenomenon that allows the material to return to its original shape under certain conditions. One of such conditions is to heat the SMA to enter in the phase transformation process, which is between the martensite phase (low temperature) and the austenite phase (high temperature). Due to this effect, SMA material can be used as an actuator, capable of transforming electrical energy into mechanical work. This material has other important features for its use as an actuator, such as high force-to-weight ratio, small volume – SMA shows one of the highest work densities at $10 Jcm^{-3}$, and ability to lift more than 100 times its weigh–. In addition, this material has a noiseless operation. At the same time, the flexibility of a SMA actuator allows to build and actuate components with different configurations and shapes adaptable to the final application. Due to its characteristics, this type of actuator was successfully used as an alternative to conventional actuators inserted in different devices, such as an elbow joint exoskeleton [26], a soft hand exo-muscular system to assist astronauts during extravehicular activities [27], a soft robotic arm inspired by the octopus [28], and in different robotics, medical, aerospace and automotive applications [29].

This research is focused on the development of a soft robotic neck with a parallel configuration, actuated by SMA-based actuators. To the best of our knowledge, there is no other SMA-based soft robotic neck in the literature. Compared to other solutions of the state of the art, our approach's contributions are:

- The prototype is softer thanks to the soft nature of the SMA actuators.
- A strong weight reduction is achieved thanks to the lightweight characteristic of the actuators.
- Motion noise is drastically reduced due to the lack of gear boxes, housing and bearings commonly used in conventional actuators.
- Different configurations of the SMA actuator can be proposed (we can change the number of SMA wires of the actuator), which makes the design more robust and versatile.
- All the previous characteristics contribute to the achievement of a real bio-inspired solution.

This article is divided into five sections. Section II presents the methodology with a description of the actuator characteristics, the design of the actuators and the proposed design for the neck platform. Section III provides the details of the control strategy, and Section IV presents the simulation and experimental results from the performance of the real neck. Section V introduces some conclusions and future works.

II. METHODOLOGY

This section briefly describes the main actuator features, SMA wire specifications and the actuator structure. The proposed neck platform design and electronic hardware are also presented.

A. SMA-BASED ACTUATOR

SMA is a metallic alloy, usually a combination of nickel and titanium, or Nitinol [30]. We can also find a combination of Nitinol with other metals, a situation that changes the properties of the actuator [31]. This material has the property of ''remembering'' its original shape, due to the SME, after heating between the two transformation phases: martensite and austenite. In this experiment, we are using the operating principle of this actuator, based on the heating process obtained as Joule effect. First, electric energy is transformed into thermal energy due to the Joule effect and then, thermal energy is transformed into mechanical work due to the properties of SMA. This type of material can be found in different configurations and shapes: wires, springs, ribbons; with different dimensions and activation temperatures (see Table 1 for the characteristics of Dynalloy wires) [30]. For the neck platform, according to characteristics such as the necessary force, displacement and work frequency, we chose the Dynalloy wire Flexinol®. We used a Flexinol wire, with a diameter of 0.51 mm, an activation temperature of $90°C$ and a nominal force of 35.6 N (with a lifetime of tens of millions of cycles in these conditions). This wire can exert a maximum force of 118 N, but it has a lifetime of hundreds or even a few thousand cycles.

The proposed SMA-based actuator consists of a SMA wire, a Bowden cable, a Polytetrafluoroethylene (PTFE) tube, and the terminal parts. The total force of the actuator can easily be modified without changing the actuator structure, simply by adding a wire in parallel with the existing wire inside the PTFE tube. This PTFE tube can accept up to 5 SMA wires with a diameter of 0.51 mm, which can add up to a nominal force of 178 N. This change will not affect the final design of the device. The structure of the actuator (Figure 1) is detailed below:

TABLE 1. SMA wires characteristics [30].

Diameter Size (mm)	Force (N)	Cooling Time 70°C (s)	Cooling Time 90°C (s)
0.025	0.0089	0.18	0.15
0.038	0.02	0.24	0.2
0.050	0.36	0.4	0.3
0.076	0.80	0.8	0.7
0.100	1.43	1.1	0.9
0.130	2.23	1.6	1.4
0.150	3.21	2.0	1.7
0.200	5.70	3.2	2.7
0.250	8.91	5.4	4.5
0.310	12.80	8.1	6.8
0.380	22.50	10.5	8.8
0.510	35.60	16.8	14.0

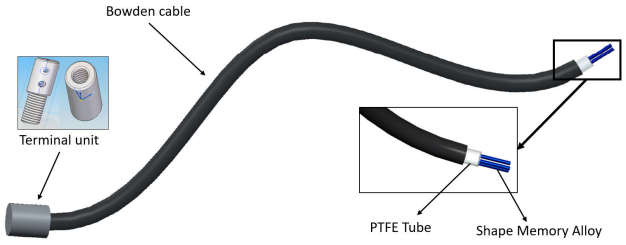

FIGURE 1. Flexible SMA-based actuator [32].

- Bowden cable. It is a metallic spiral covered with a nylon sheath. Its objective is the transmission of force, giving the flexibility advantage of the actuator at the same time. It also helps dissipate the heat when the SMA wire is in the cooling stage (recovering the initial length).
- PTFE tube. It is placed between the SMA wires and the Bowden cable, and acts as an electrical insulator. In addition, this type of material is considered a solid lubricant, preventing friction between the wires and the tube shell. It can also work at high temperatures, over 250°C.
- SMA wires. The actuator is made up of one or more SMA wires whose diameter and length are calculated according to the necessary force and the final displacement of the device.
- Terminal units. They are used to fix the SMA wires with the Bowden cable, at one end, and the SMA wire with the actuated system or the tendons of the actuated system, at the opposite end. Furthermore, those terminal units are used as connectors for power supplying the actuator.

It is important to remark that, during the actuation, the Bowden cable and the PTFE tube do not change their volume or dimensions and do not displace with the SMA wire. The only part of the actuator that shows displacement is the SMA wire.

Our research group already presented in [32] an analysis of different configurations of SMA actuators with one or more SMA wires and the effect of the Bowden cable on the structure of the actuator. In this experiment we have chosen to use an actuator based on one SMA wire, a PTFE tube and a Bowden cable.

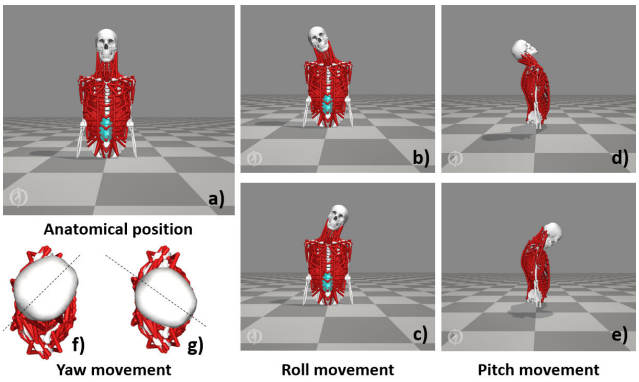

FIGURE 2. Human neck motions (obtained with OpenSim [35]): a) Anatomical position of the human body; b) and c) lateral bending or roll movement; d) neck extension and f) neck flexion - these two movements represent the pitch movement; g) and h) vertical rotation or yaw movement.

B. SOFT NECK PLATFORM

The human neck has three DOF that allow for flexion/extension (pitch), vertical rotation (yaw), and lateral flexion (roll) [33]. These movements can be seen in Figure 2. Each movement, according to anatomical position, corresponds to: 45° for lateral flexion (Figure 2b and c), 57.5° for extension movement (Figure 2d), 50° for flexion movement (Figure 2e), and around 70° for vertical rotation (Figure 2f and g) [34].

The proposed soft neck platform is based on the solution presented in the publications ''Design and performance validation of a cable-driven soft robotic neck'' [34] and ''Test Bench for Evaluation of a Soft Robotic Link'' [36]. This is a parallel platform with two DOF (pitch and roll) that becomes a more reliable approach to a biological inspired human neck. With some modifications to the static base, one more actuator can be added for the yaw movement. Different from these previous papers, this work focuses on the pitch and roll movement of the neck through the integration and actuation of SMA- based actuators. The resulting solution is a low-cost platform manufactured with a 3D printer, which includes low-cost electronics and actuators. The platform presents a minimum number of rigid parts, being considered a flexible and soft prototype with low weight and noiseless operation. The robotic neck consists of two 3D printed fixed platforms of polylactic acid (PLA) material: one platform supports the base of the prototype and the other fixes the Bowden cable. The robotic neck also has a 3D printed central column of FilaFlex material, a 3D printed mobile platform of PLA material, three tendons and three SMA-based actuators. The platform of the structure is shown in Figure 3. The central column has some flexibility - a shape inspired by the human spine, with 5 vertebrae. This platform is a proof of concept and its maximum payload is limited by the central column. The maximum payload can be modified by changing the column thickness and the printing density. In this experiment, the vertical column has a maximum diameter of 20 mm and was printed with a 30% density. With those

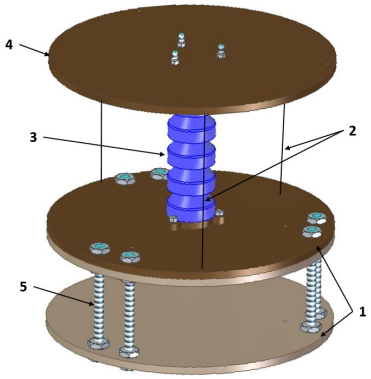

FIGURE 3. CAD model of the neck structure platform.

TABLE 2. Neck platform characteristics.

Parameter	Value	Unit
Diameter of bases	0.09	m
Length of neck column	0.1	m
Maximum diameter of neck column	0.02	m
FilaFlex Density	1.2	g/cm^3
FilaFlex Young's Modulus	15.2	MPa
FilaFlex Poisson's Ratio	0.48	
FilaFlex Damping constant	0.005	

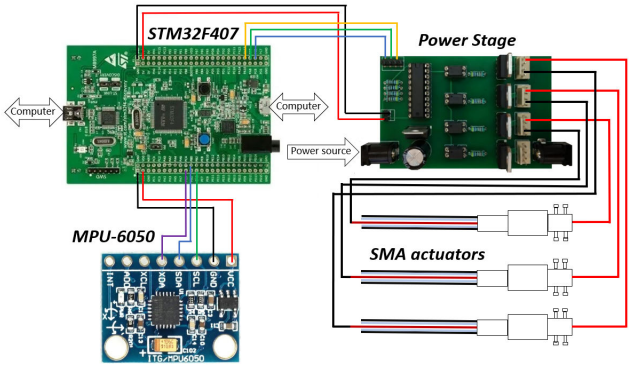

FIGURE 4. Electronic connections.

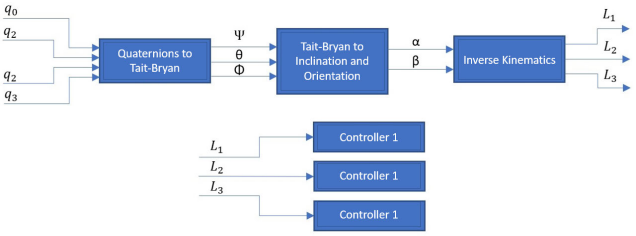

FIGURE 5. Data process steps.

parameters, the current platform can support more than 1 kg of payload. We can increase the maximum payload to 5 kg by reprinting the spine and changing the actuators. The proposed mechanism, based on three tendons, allows two DOF (pitch and roll movements) with a maximum angle of 40 degrees for inclination and 360 degrees for orientation.

Figure 3 shows the Computer Aided Design (CAD) structure of the neck platform where:

- Element 1- fixed bases. The SMA-based actuators will be placed between these two bases;
- Element 2- tendons (nylon fishing wire with a diameter of 0.8 mm and a maximum force of 180 N, manufactured by Caperlan);
- Element 3- neck column;
- Element 4- flexible base;
- Element 5- screws that separate the fixed bases. They keep the bases separated at a distance of 50 mm.

The main characteristics and dimensions of the neck platform including the spine are shown in Table 2.

C. ELECTRONIC HARDWARE

The electronic hardware of the neck platform consists of an inertial sensor, a microcontroller and a power circuit required to control the SMA-based actuators. The electronic connections between those components are shown in Figure 4. The inertial sensor, MPU-6050 from Paradisetronic [37], is used as a gyroscope, obtaining the instantaneous quaternion values (via Inter-Integrated Circuit (I^2C) bus) that, through a series of conversions, serve as a feedback for the controller loop. This low-cost sensor model was chosen because of its small dimensions and its ability to easily integrate into the system. It was placed in the center of the mobile platform.

The electronic power circuit for SMA wires is based on MOSFET transistors. The transistors are activated by Pulse Width Modulation (PWM) provided by the controller. The transistors open and close the circuit with a power supply for the actuators. With these electronics (developed by our research group), the control hardware architecture is capable of managing four different actuators (each actuator with one or more SMA wires).

The controller board is based on the STM32F407 Discovery kit [38], from STMicroelectronics, which is programmed with Matlab/Simulink® [39]. This manages signals from the sensors, executes the control algorithm for controlling the actuators, and generates the required PWM signals.

III. CONTROL

To control the neck platform, the tendon lengths must be extracted by processing the data from the IMU sensor. Tendon lengths are used to calculate the movements of the actuator. First, the quaternions must be transformed into Tait-Bryan angles. With these angles, we can easily build the rotation matrix and obtain the orientation and inclination parameters, which will also be used to indicate the desired neck position. The last step is to apply inverse kinematics to convert the orientation and inclination angles into tendon lengths. The steps are shown in Figure 5, where q_i are the quaternions, ϕ, θ and ψ are the Euler angles, α and β are the inclination and orientation angles of the robotic neck, and L_i is the tendon length, which is used to calculate the movement of the actuator.

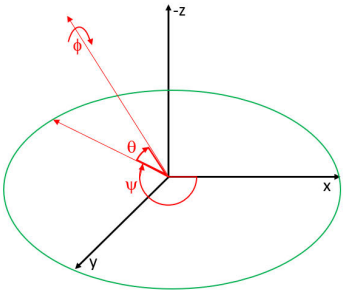

FIGURE 6. Yaw, pitch and roll angles representation in xyz.

A. ANGLE TRANSFORMATION

The first step involves representing the quaternions obtained from the inertial sensor at Tait-Bryan angles and Euler angles in terms of flight dynamics (equation 1). Euler angles can be obtained directly from the sensor, however the use of quaternions avoids singularities that prevent improper operation. Tait-Bryan is used because at the starting point, when the neck rests horizontally, the angle would be 0°.

$$\begin{bmatrix}\phi\\ \theta\\ \psi\end{bmatrix} = \begin{bmatrix}atan2(2(q_0q_1+q_2q_3), 1-2(q_1^2+q_2^2))\\ asin(2(q_0q_2+q_3q_1))\\ atan2(2(q_0q_3+q_1q_2), 1-2(q_2^3+q_3^2))\end{bmatrix} \quad (1)$$

The base change matrix of the rotated system (equation 2, where roll (ϕ), pitch (θ), and yaw (ψ) are as in Figure 6), is used to convert Tait-Bryan angles into orientation and inclination angles:

$$R_{\phi,\psi,\theta} = \begin{bmatrix}c\psi c\theta & c\psi s\theta s\phi - s\psi c\phi & c\psi s\theta c\phi + s\psi s\phi\\ s\psi c\theta & s\psi s\theta s\phi + c\psi c\phi & s\psi s\theta c\phi - c\psi s\phi\\ -s\theta & s\phi c\theta & c\theta c\phi\end{bmatrix} \quad (2)$$

where s is *sin* and c is *cos*.

We will just take R_θ, and cancel R_ψ ($\psi = 0$) because it is unnecessary since the neck platform has only two DOF, where θ is inclination and ϕ orientation. Therefore, the rotation matrix was reduced by a vector [36]:

$$R_{TB} = \begin{bmatrix}s\theta c\phi\\ -s\phi\\ c\theta c\phi\end{bmatrix} \quad (3)$$

The angle of inclination α is the projection of the vector R_{TB} on the Z-axis, described by equations 4 and 5:

$$\cos\alpha = \frac{R_{TB}^{\intercal}\cdot Z}{||R_{TB}||\cdot||Z||} = \frac{\begin{bmatrix}s\theta c\phi\\ -s\phi\\ c\theta c\phi\end{bmatrix}^{\intercal}\cdot\begin{bmatrix}0\\0\\1\end{bmatrix}}{||R_{TB}||\cdot||Z||} \quad (4)$$

$$\cos\alpha = \frac{c\theta c\phi}{\sqrt{(s\theta c\phi)^2+(-s\phi)^2+(c\theta c\phi)^2}} \quad (5)$$

The angle of orientation β is the projection of vector R_{TB} on the XY plane. The solution can be found using the projection

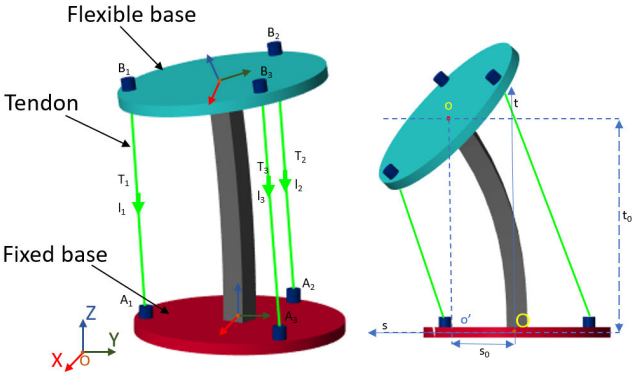

FIGURE 7. Neck platform kinematics: left– cable driven parallel mechanism; right– lateral bending of the mobile platform.

on the X axis, with equations 6 and 7:

$$\cos\beta = \frac{R_{TB}^{\intercal}\cdot X}{||R_{TB}||\cdot||X||} = \frac{\begin{bmatrix}s\theta c\phi\\ -s\phi\\ c\theta c\phi\end{bmatrix}^{\intercal}\cdot\begin{bmatrix}1\\0\\0\end{bmatrix}}{||R_{TB}||\cdot||X||} \quad (6)$$

$$\cos\beta = \frac{s\theta c\phi}{\sqrt{(s\theta c\phi)^2+(-s\phi)^2+(c\theta c\phi)^2}} \quad (7)$$

B. INVERSE KINEMATICS

The kinematics of the neck platform was calculated based on Nagua *et al.* [34]. The lengths of each tendon can be calculated using the angles of orientation (β) and inclination (α), previously obtained in Section III-A.

According to Figure 7 (left), two coordinate bases are assumed, one formed by *OXYZ* placed on the fixed structure (red platform) and another one formed by *oxyz* on the mobile platform (green platform). The axes are referenced so that Z and z are perpendicular to their respective platforms in a positive way and with the same direction.

A_i is the set of points through the SMA wires pass in the fixed base and B_i is the set of points in the mobile base where the tendons are attached. The tendon length is the distance between A_i and B_i.

In the plane formed by the points O, o' and o (Figure 7 right side, a new two-dimensional coordinate base is created formed by the axis t and s. The *t-axis* has the same direction as Z, and the *s-axis* has the direction of Oo'.

- θ_s is the angle created between *s-axis* and *X-axis*.
- θ_p is the angle formed after the mobile platform rotation on itself.
- t_o is the distance between points O and o following the *t-axis*.
- s_o is the distance between points O and o following the *s-axis*.

Using the Tait-Bryan angles we find the rotation matrix ${}^{o}R_{o'}$ (Section III-A) used to calculate the orientation and inclination angles. ${}^{o}T_{o'}$ is the homogeneous transformation matrix that represents the projection of *oxyz* on *OXYZ*, described by

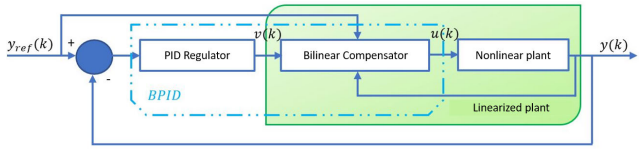

FIGURE 8. BPID controller.

the equation 8:

$$ {}^{o}T_{o'} = \begin{bmatrix} {}^{o}R_{o'} & P_o \\ 0 & 1 \end{bmatrix} \tag{8} $$

where P_o is the position vector of point o according to the base coordinate and described by the equation 9:

$$ P_o = \begin{bmatrix} s_o \cos\theta_s & s_o \sin\theta_s & t_o \end{bmatrix}^{\mathsf{T}} \tag{9} $$

According to this, the tendon lengths can be calculated, using the equation 10:

$$ L_i = ||{}^{o}T_{o'}\overrightarrow{oB_i} - \overrightarrow{OA_i}|| \tag{10} $$

where $\overrightarrow{oB_i}$ represents the points where the tendons are fixed on the mobile platform and $\overrightarrow{OA_i}$ represents the points where the tendons are fixed on the base.

Once all the variable changes and hence the length of tendons have been obtained, the controller can be implemented.

C. BPID CONTROLLER

A type of bilinear controller consisting of a conventional Proportional Integral Derivative (PID) controller, in cascade with a bilinear compensator, known as Bilinear Proportional Integral Derivative (BPID) controller, was proposed to control the soft robotic neck. The bilinear compensator is a subset of non-linear controllers. This represents a promising alternative to cancel the non-linear behavior due to the thermal hysteresis of the SMA-based actuator, when this is controlled in position. This control technique is simpler and easier to implement compared to other non-linear control strategies and it was successfully used in the control of SMA actuators [26], [40]. The performance of the BPID controller was demonstrated by comparing its response to the response of other two controllers – a conventional PID and a commuted feed forward PIPD –, while controlling a real SMA actuator [41]. The scheme of the BPID controller is shown in Figure 8, where: $y_{ref}(k)$ is the reference value of the wire displacement, $y(k)$ is the wire position displacement value received from the IMU sensor already transformed into the tendon length displacement, $v(k)$ is the control signal created by the PID controller and $u(k)$ is the signal rectified with the bilinear compensator.

The continuous state space equations as a SISO system (single-input single-output) can be represented as follows (see equation 11):

$$ \begin{cases} \dot{x}(t) = Ax(t) + Bu(t) + u(t)Nx(t) \\ y(t) = Cx(t), \end{cases} \tag{11} $$

TABLE 3. BPID controller gains.

Gain	Kp	Kd	Ki	Kb
Value	24	0	10	2

where x is the state vector, $u(t)$ the input, A a nxn matrix, B a $nx1$ matrix, C a $1xn$ matrix, N a nxn matrix and $y(t)$ the output.

The discrete equation (with a sample time of 0.002 s) (equations 12, 13) of the bilinear compensator is as follows:

$$ \frac{U(z)}{V(z)} = \frac{1 + k_b Y_{ref}(z)}{1 - k_b z^{-1} Y(z)}, \tag{12} $$

$$ I(z) = [k_p + k_i T_s \frac{1}{z-1} + k_d \frac{N}{1 + NT_s \frac{1}{z-1}}]E(z). \tag{13} $$

Gain values have been found according to the SMA actuator model, presented in [42], available at Matlab/Simulink®, and connected with the dynamic model of the neck platform (presented in section IV-A). The dynamic model of the neck platform was modified to receive the tendon displacement as a reference. The first output of this model consists of the quaternion which is transformed with the inverse kinematics in tendon displacement. The second output consists of the force necessary for this displacement. This modified model was connected in series with the SMA actuator model (SMA model after the neck platform model), and the control loop was closed with the position signal. The BPID parameters obtained in Matlab® with this model were used during the tests and are shown in Table 3.

IV. SIMULATIONS AND EXPERIMENTS

This section presents the neck platform simulation and experimental results of the prototype.

A. NECK PLATFORM SIMULATION

Matlab/Multibody® software was used to develop the neck dynamic model, using the characteristics of the neck platform described in Section II-B. When we developed this model, we used blocks such as bodies, a flexible cylindrical beam and wires from the Simscape library. Those blocks were configured according to the parameters of the neck platform. The interface created with this software is shown in Figure 7. The model accepts the force of the actuators as an input signal, and is used to return the positions of the cables (as output signals) to match the displacement of the actuator. In addition, the mobile platform block was configured to return the quaternion data (from the center of the platform) according to the base. These data can be used to calculate the length of the cables using angle transformation and inverse kinematics (as described in Section III).

According to the simulation, to obtain 40 degrees of neck inclination, the actuator needs a displacement of 0.051 m. In this experiment we chose three SMA-based actuators with a length of 1.7 m each, considering that in the inclination movement one actuator is activated while, at the same

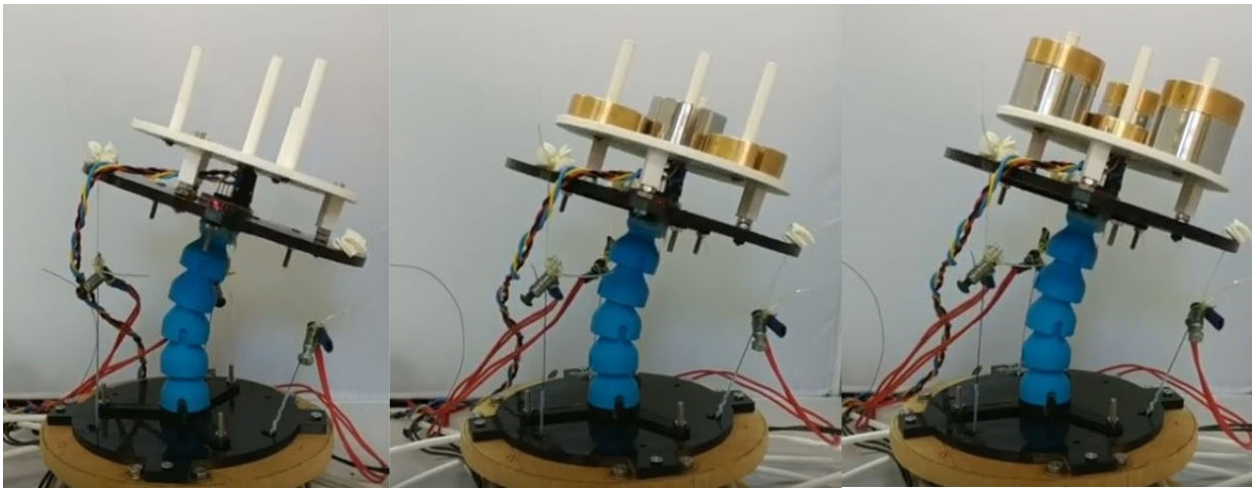

FIGURE 9. Neck platform actuated with different payloads.

time, another actuator on the opposite side of the platform has to expand to leave the system free. The characteristics of the SMA-based actuators are 90 °C activation and 4% stroke from its total length. With such dimensions the actuator has a maximum movement of 0.068 m, which will be enough for the desired robotic neck movement. In this way, by over-sizing the actuator, we prevent the maximum heating of the actuator, and the cooling and stretching of the material is faster. Assuming that the resistance of the wires is $4.3\Omega/m$ and the operating energy consumption is 4 A (Table 1), the calculated voltage supply was 29 V.

B. RESULTS

The proposed test to evaluate the developed platform consists of performing two laps with two different inclinations each. One lap means varying the orientation degrees from 0 degrees to 360 degrees, changing at 10 degrees per second. During the first lap, the neck will be tilted 10 degrees. For the second lap, the tilt value will change to 20 degrees. With this set-up, we performed three tests. First, the neck will only be subjected to the support weight. In the second test, three weights of 0.1 kg each and one of 0.2 kg, for a total of 0.5 kg, were placed on the neck platform; and for the last test four weights of 0.1 kg each and three weights of 0.2 kg each, for a total of 1 kg, were placed. The neck platform with these different payloads is shown in Figure 9. The weights were placed by attaching a four-cylinder base to the mobile platform (see the white piece in Figure 9).

The control algorithm was configured so that the neck platform performs a smooth movement very similar to the movements of the human neck. The robotic neck complies with the speed ranges of the human neck, although speed in the antagonist configuration is a major issue in this type of actuators. Due to the antagonistic configuration of the actuators, we consider the temperature of the actuators and the antagonistic tensions to be important parameters. According to the SMA technical specifications, Table 1, the SMA wire needs 14 seconds to recover its initial shape. The wire from the opposite side does not need to reach the maximum contraction within those 14 seconds. In this case, the maximum speed of one lap cannot exceed 28 seconds/lap if the neck performs a continuous rotational movement at a constant speed. If the neck movement is not a continuous rotation and it is only a point movement (i.e. flexion), the neck platform does not have a speed limit, but we cannot activate both actuators at maximum at the same time. We must wait few seconds between stopping the first actuator and activating the second one.

To compare the neck speeds of healthy humans with the results obtained in this experiment, we used Cheng *et al.* [43] research. The measurement of the healthy subject, revealed different types of speed. Those speeds were measured for flexion, extension and left/right lateral bending, they were classified in three categories and ranged approximately from 23 to 34°/s for fast speed, from 7.9 to 13.1°/s for medium speed and from 3.0 to 4.4°/s for slow speed. Even if the antagonistic forces affect the speeds of the neck platform, this is capable of reaching all of these speeds. The only limitation is when maximum movement is requested to two opposite actuators: if one actuator is activated to maximum (i.e. flexor), the opposite actuator (i.e. extensor) should be activated only after a few seconds from the time of deactivation of the first actuator (flexor), because this first actuator needs some time to cool down. The required cooling time depends on the payload and the total displacement. If the actuator does not perform the maximum displacement, the temperature of the SMA wires is lower and they take less time to recover their initial form. In the same way, the larger the payload of the platform, the higher temperature of the wire. However, this platform is designed as a prototype concept, to demonstrate the feasibility of a soft and bio-inspired system, where the actuators can be configured according to the final application. For example, we can use multi-wire actuators [32] with a smaller diameter (Table 1) for fast cooling or actuators with

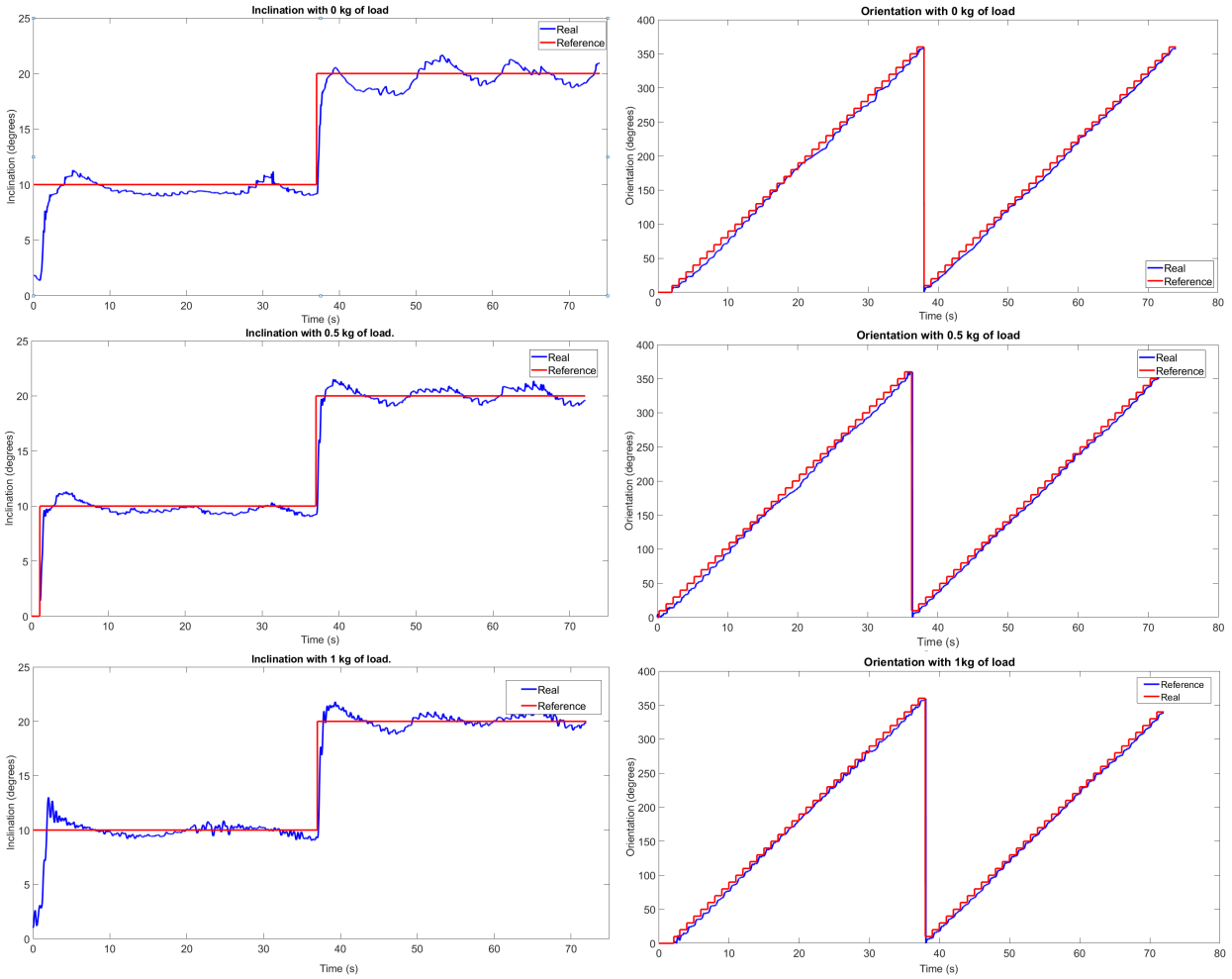

FIGURE 10. Neck inclination and orientation with different payloads.

multiple wires and the same diameter (0.51 mm) to increase the total force of the platform, without changing the structure of the neck platform.

Some tests were carried out and the most relevant data were collected to compare the actual positions of the neck platform with the references. The orientation, inclination, wire length (displacement) and PWM signals of each actuator were acquired using Matlab®. These data help us analyze the performance of the controller and the proposed platform.

Figure 10 shows the neck platform response to different payloads. The inclination tracks a step signal with two amplitudes: first – 10 degrees and, after 36 seconds, it changes to 20 degrees of inclination. In these 36 seconds, the neck platform has done a complete lap (360-degree orientation movement). As Figure 10 shows, the loads affect the response of the neck platform. With no payload or with light weights the response presents more oscillations around the reference signal. With heavy loads (e.g. 1 kg) these oscillations are reduced. On the other hand, with a payload of 1 kg, the system presents an overshoot that is apparent. However, the maximum error in the permanent stage is less than 2 degrees.

On the right side of Figure 10, we can observe the orientation movement of the neck, the platform tracks the reference signal quite accurately. The reference signal is generated every second with microsteps of 10°/s, in total a complete lap of 360 degrees in 36 seconds. Although in this movement the platform does not have enough time to reach the permanent stage, the error at the end of each micro step is less than 1 degree. The controller can be reconfigured for faster response but in this case the reference must be generated more precisely (each step less than 10 degrees) for a smooth movement. On the contrary, the movement will be interrupted.

The movements of inclination and orientation are generated by the actuator activation that converts the wire length to orientation/inclination displacement (for the actuation) and vice versa (from the inertial sensor, data is converted to wire length — the feedback for the control loop). Figure 11 shows how the length of the tendon wire varies according to the references generated in Figure 10. In this article we only analyze the length of tendon 1 with different payloads on the neck platform, since responses of other actuators were

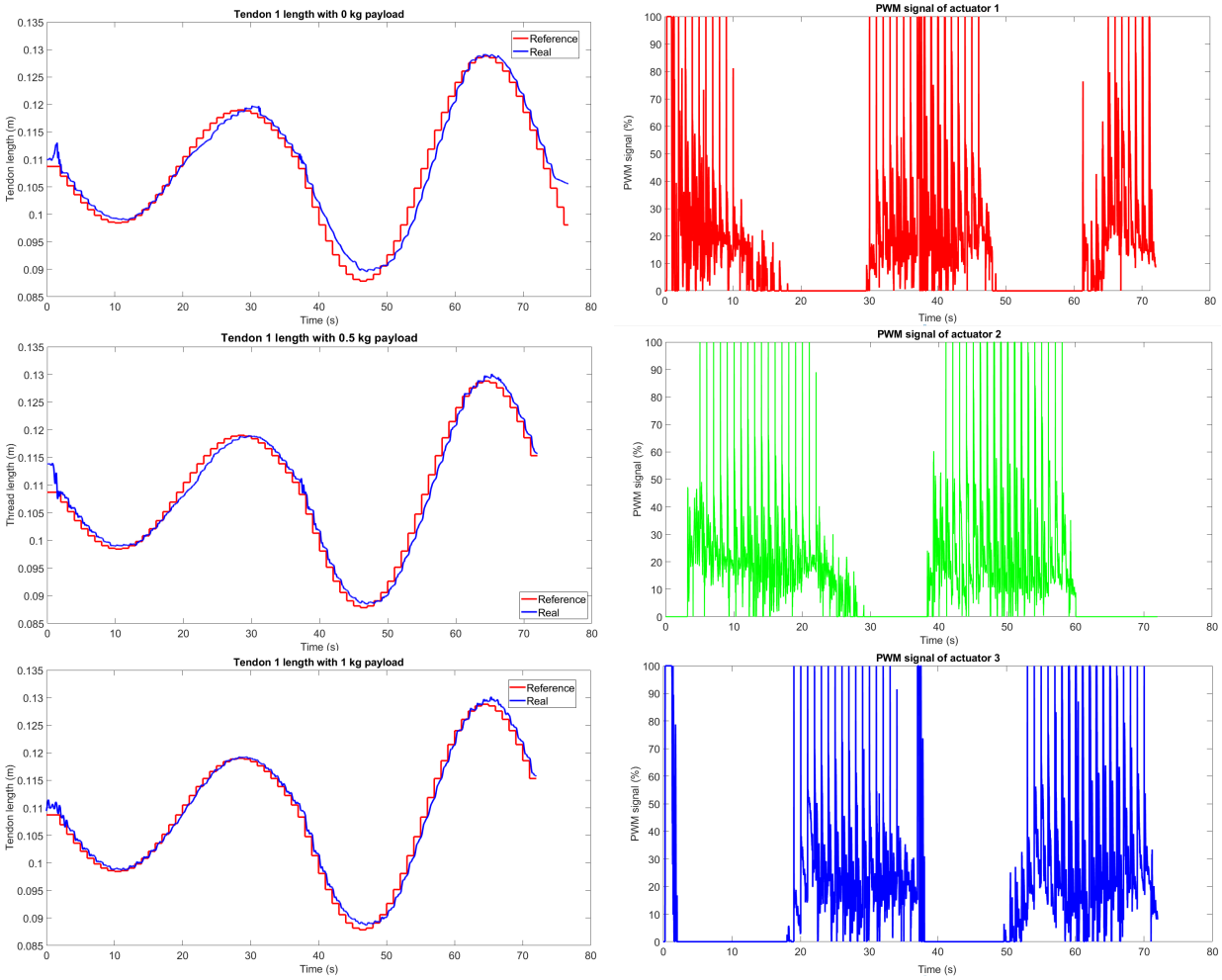

FIGURE 11. Length of tendons with different payloads (on the left) and the PWM signals of the 3 actuators with 0.5 kg of payload (on the right).

similar and they were considered irrelevant to be analyzed separately.

Looking closely, larger errors are observed when the platform has no payloads. As weights are added, the results improve in terms of average error, obtaining better approximations between the real curve and the reference with small difference. Even if there is a problem with some oscillations, the platform with the payloads properly tracks the reference, and its response can be improved by reconfiguring the controller.

On the right side of Figure 11, the PWM signals of the three actuators are presented when the neck platform has a payload of 0.5 kg and moves according to the references presented in Figure 10. PWM signals are alternatively activated (antagonistic mode) to produce the desired movement (never more than two actuators) for example, in the first instance, the actuators 1 and 3 are activated to move the neck platform from 0 degrees to 10 degrees inclination while maintaining 0 degrees of orientation. Progressively, actuator 3 is deactivated and actuator 2 is activated to change the orientation according to the reference. According to this operating mode, the electrical power never exceeds 234 W at the peak of consumption. Peaks at 100% of PWM are generated when the reference is changed (micro steps) and errors increase.

The neck platform developed in this experiment was compared to the soft neck platform developed by Mena *et al.* [36]. From the point of view of total weight (neck platform with its actuators and drivers) the robotic neck presented by Mena *et al.* [36] uses Maxon motors – Maxon RE 35; graphite brushes, 42 Volt, 90 Watt – along with a planetary gear – Maxon planetary gearhead GP32A (3.7: 1) – whose total weight (motor and gear) is around 0.53 kg. This means that the actuators have a total weight of 1.59 kg to which the weight of the drivers, bases, and the spring (0.1 kg) used such vertical column is added. In our case, using the SMA-based solution where each actuator has a weight of 0.1 kg (a total of 0.3 kg), we managed to reduce the total weight of the neck platform significantly. The total weight of the actuator is largely due to the Bowden cable. On the other hand, due to the flexibility of the actuator, only the bases are rigid, the rest of components are flexible and made of soft materials. Both soft neck platforms can be manufactured using a 3D printer, which

reduces the costs. Besides, the SMA-based actuators are a considerably cheaper alternative to the conventional motors used by Mena *et al.* [36]. In terms of performance control, both platforms have similar results and are able to reach different orientation and inclination positions. In the case of Mena *et al.* [36], with payloads close to 1 kg, the behavior of the system is close to instability, an effect that was not detected in our system. Depending on the payload and the displacement of the actuator, our neck platform may have a speed limitation, but this can be improved by reconfiguring the actuator or adding an external cooling system. If the movement is not a continuous lap, this limitation does not exist, but the behavior of the neck platform depends on the rules of the antagonistic movement. For example, it is not possible to actuate two opposite actuators simultaneously in the same direction with reference signals that are not possible from the point of view of actuator movements (contracting two opposite actuators to the maximum). The SMA-based actuators are less energy efficient compared to conventional actuators. Regarding operation noise, our neck platform is quieter, and can be considered noise-free.

V. CONCLUSION

In this article we introduced a soft robotic neck actuated by SMA actuators, which, compared to existing robotic necks actuated by conventional motors has the advantage of low weight (the weight of the whole structure with the actuators and hardware is less than 0.5 kg), noiseless operation and low-cost development. The characteristics of these actuators with the proposed structure make the robotic neck a biological-inspired system, very close to human neck behavior. With this work, we validate the fact that the developed neck platform has a similar behavior to the human neck and can reproduce most movements with similar speeds.

The flexible SMA-based actuator is a nonlinear system with high hysteresis that requires the use of nonlinear control methods. In this work, a BPID controller was used to improve the behavior of the SMA-based actuators response. The neck platform maintained the desired inclination position (with a maximum error of 2 degrees) while, at the same time, it followed the orientation movement reference.

The proposed robotic neck has a minimum of rigid parts (only the bases), the remaining components are soft, with a flexible actuator that can move a payload of up to 1 kg. This preliminary design can be considered one step ahead to the development of really soft robotic platforms.

As a future work, new actuators configurations will be addressed (for example, the use of two small diameter SMA wires in parallel) and a possible artificial cooling system based on air flow will be added to improve the actuator cooling process.

REFERENCES

[1] M. Nordin and V. Frankel, *Basic Biomechanics of the Musculoskeletal System*. New York, NY, USA: Lippincott Williams & Wilkins, 2001.

[2] L. Nagua, J. Munoz, C. A. Monje, and C. Balaguer, "A first approach to a proposal of a soft robotic link acting as a neck," in *Proc. 39th Actas de las Jornadas de Automática*, Badajoz, Spain, 2018, pp. 5–7.

[3] Y. Sakagami, R. Watanabe, C. Aoyama, S. Matsunaga, N. Higaki, and K. Fujimura, "The intelligent ASIMO: System overview and integration," in *Proc. IEEE/RSJ Int. Conf. Intell. Robots Syst.*, vol. 3, Sep. 2002, pp. 2478–2483.

[4] I.-W. Park, J.-Y. Kim, J. Lee, and J.-H. Oh, "Mechanical design of humanoid robot platform KHR-3 (KAIST humanoid robot–3: HUBO)," in *Proc. 5th IEEE-RAS Int. Conf. Humanoid Robots*, Dec. 2005, pp. 321–326.

[5] K. Kaneko, F. Kanehiro, M. Morisawa, K. Akachi, G. Miyamori, A. Hayashi, and N. Kanehira, "Humanoid robot HRP-4–Humanoid robotics platform with lightweight and slim body," in *Proc. IEEE/RSJ Int. Conf. Intell. Robots Syst.*, Sep. 2011, pp. 4400–4407.

[6] D. Gouaillier, V. Hugel, P. Blazevic, C. Kilner, J. Monceaux, P. Lafourcade, B. Marnier, J. Serre, and B. Maisonnier, "Mechatronic design of NAO humanoid," in *Proc. IEEE Int. Conf. Robot. Autom.*, May 2009, pp. 769–774.

[7] J. Englsberger, A. Werner, C. Ott, B. Henze, M. A. Roa, G. Garofalo, R. Burger, A. Beyer, O. Eiberger, K. Schmid, and A. Albu-Schaffer, "Overview of the torque-controlled humanoid robot TORO," in *Proc. IEEE-RAS Int. Conf. Humanoid Robots*, Nov. 2014, pp. 916–923.

[8] A. K. Pandey and R. Gelin, "A mass-produced sociable humanoid robot: Pepper: The first machine of its kind," *IEEE Robot. Autom. Mag.*, vol. 25, no. 3, pp. 40–48, Sep. 2018.

[9] M. Penčić, M. Čavić, S. Savić, M. Rackov, B. Borovac, and Z. Lu, "Assistive humanoid robot marko: Development of the neck mechanism," in *Proc. MATEC Web Conf.*, vol. 121. Les Ulis, France: EDP Sciences, 2017, Art. no. 08005.

[10] D. Hayosh, X. Liu, and K. Lee, "Woody: Low-cost, open-source humanoid torso robot," in *Proc. 17th Int. Conf. Ubiquitous Robots (UR)*, Jun. 2020, pp. 247–252.

[11] M. K. Mallick and A. Sudheer, "Kinematic and static structural analysis of a humanoid with a wheeled mobile base," in *Proc. Innov. Product Design Intell. Manuf. Syst.* Singapore: Springer, 2020, pp. 991–1001.

[12] J.-H. Oh, D. Hanson, W.-S. Kim, Y. Han, J.-Y. Kim, and I.-W. Park, "Design of Android type humanoid robot albert HUBO," in *Proc. IEEE/RSJ Int. Conf. Intell. Robots Syst.*, Oct. 2006, pp. 1428–1433.

[13] K. Kaneko, F. Kanehiro, M. Morisawa, K. Miura, S. Nakaoka, and S. Kajita, "Cybernetic human HRP-4C," in *Proc. 9th IEEE-RAS Int. Conf. Humanoid Robots*, Dec. 2009, pp. 7–14.

[14] R. Beira, M. Lopes, M. Praca, J. Santos-Victor, A. Bernardino, G. Metta, F. Becchi, and R. Saltaren, "Design of the robot-cub (iCub) head," in *Proc. IEEE Int. Conf. Robot. Autom. (ICRA)*, May 2006, pp. 94–100.

[15] K. Berns and J. Hirth, "Control of facial expressions of the humanoid robot head ROMAN," in *Proc. IEEE/RSJ Int. Conf. Intell. Robots Syst.*, Oct. 2006, pp. 3119–3124.

[16] Y. Tadesse, K. Subbarao, and S. Priya, "Realizing a humanoid neck with serial chain four-bar mechanism," *J. Intell. Mater. Syst. Struct.*, vol. 21, no. 12, pp. 1169–1191, Aug. 2010, doi: 10.1177/1045389X10378775.

[17] N. Pateromichelakis, A. Mazel, M. A. Hache, T. Koumpogiannis, R. Gelin, B. Maisonnier, and A. Berthoz, "Head-eyes system and gaze analysis of the humanoid robot romeo," in *Proc. IEEE/RSJ Int. Conf. Intell. Robots Syst.*, Sep. 2014, pp. 1374–1379.

[18] I. Mizuuchi, R. Tajima, T. Yoshikai, D. Sato, K. Nagashima, M. Inaba, Y. Kuniyoshi, and H. Inoue, "The design and control of the flexible spine of a fully tendon-driven humanoid 'Kenta,'" in *Proc. IEEE/RSJ Int. Conf. Intell. Robots Syst.*, vol. 3, Sep. 2002, pp. 2527–2532.

[19] Y. Nakanishi, Y. Asano, T. Kozuki, H. Mizoguchi, Y. Motegi, M. Osada, T. Shirai, J. Urata, K. Okada, and M. Inaba, "Design concept of detail musculoskeletal humanoid 'kenshiro' toward a real human body musculoskeletal simulator," in *Proc. 12th IEEE-RAS Int. Conf. Humanoid Robots (Humanoids 2012)*, Nov. 2012, pp. 1–6.

[20] Y. Asano, K. Okada, and M. Inaba, "Design principles of a human mimetic humanoid: Humanoid platform to study human intelligence and internal body system," *Sci. Robot.*, vol. 2, no. 13, Dec. 2017, Art. no. eaaq0899. [Online]. Available: https://robotics.sciencemag.org/content/2/13/eaaq0899

[21] I. Mizuuchi, T. Yoshikai, Y. Sodeyama, Y. Nakanishi, A. Miyadera, T. Yamamoto, T. Niemela, M. Hayashi, J. Urata, Y. Namiki, T. Nishino, and M. Inaba, "Development of musculoskeletal humanoid kotaro," in *Proc. IEEE Int. Conf. Robot. Autom. (ICRA)*, May 2006, pp. 82–87.

[22] D. Cafolla, M. Wang, G. Carbone, and M. Ceccarelli, "LARMbot: A new humanoid robot with parallel mechanisms," in *Proc. Robot Design, Dyn. Control (ROMANSY)*, V. Parenti-Castelli and W. Schiehlen, Eds. Cham, Switzerland: Springer, 2016, pp. 275–283.
[23] J. Reinecke, B. Deutschmann, and D. Fehrenbach, "A structurally flexible humanoid spine based on a tendon-driven elastic continuum," in *Proc. IEEE Int. Conf. Robot. Autom. (ICRA)*, May 2016, pp. 4714–4721.
[24] B. Gao, Z. Zhu, J. Zhao, and L. Jiang, "Inverse kinematics and workspace analysis of a 3 DOF flexible parallel humanoid neck robot," *J. Intell. Robotic Syst.*, vol. 87, no. 2, pp. 211–229, Aug. 2017.
[25] A. Garriga-Casanovas, A. M. Faudzi, T. Hiramitsu, F. R. Y. Baena, and K. Suzumori, "Multifilament pneumatic artificial muscles to mimic the human neck," in *Proc. IEEE Int. Conf. Robot. Biomimetics (ROBIO)*, Dec. 2017, pp. 809–816.
[26] D. Copaci, F. Martin, L. Moreno, and D. Blanco, "SMA based elbow exoskeleton for rehabilitation therapy and patient evaluation," *IEEE Access*, vol. 7, pp. 31473–31484, 2019.
[27] Á. Villoslada, C. Rivera, N. Escudero, F. Martín, D. Blanco, and L. Moreno, "Hand exo-muscular system for assisting astronauts during extravehicular activities," *Soft Robot.*, vol. 6, no. 1, pp. 21–37, Feb. 2019, doi: 10.1089/soro.2018.0020.
[28] C. Laschi, M. Cianchetti, B. Mazzolai, L. Margheri, M. Follador, and P. Dario, "Soft robot arm inspired by the octopus," *Adv. Robot.*, vol. 26, no. 7, pp. 709–727, Jan. 2012.
[29] J. Mohd Jani, M. Leary, A. Subic, and M. A. Gibson, "A review of shape memory alloy research, applications and opportunities," *Mater. Design*, vol. 56, pp. 1078–1113, Apr. 2014.
[30] Dynalloy. (2020). *Technical Characteristics of Flexinol*. Accessed: Apr. 20, 2020. [Online]. Available: http://www.dynalloy.com/
[31] Saes. (2020). *Shape Memory Alloys/Nitinol*. Accessed: Apr. 20, 2020. [Online]. Available: https://www.saesgetters.com/products-functions/products
[32] D. Copaci, D. Blanco, and L. E. Moreno, "Flexible shape-memory alloy-based actuator: Mechanical design optimization according to application," *Actuators*, vol. 8, no. 3, p. 63, Aug. 2019, doi: 10.3390/act8030063.
[33] S. Alfayad, M. El Asswad, A. Abdellatif, F. B. Ouezdou, A. Blanchard, N. Beaussé, and P. Gaussier, "Hydroïd humanoid robot head with perception and emotion capabilities: Modeling, design, and experimental results," *Frontiers Robot. AI*, vol. 3, p. 15, Apr. 2016.
[34] L. Nagua, J. Munoz, C. A. Moñje, and C. Balaguer, "Design and performance validation of a cable-driven soft robotic neck," in *Proc. Actas de las Jornadas Nacionales de Robótica*, Alicante, Spain, Jun. 2019, pp. 13–14.
[35] J. D. Mortensen, A. N. Vasavada, and A. S. Merryweather, "The inclusion of hyoid muscles improve moment generating capacity and dynamic simulations in musculoskeletal models of the head and neck," *PLoS ONE*, vol. 13, no. 6, Jun. 2018, Art. no. e0199912.
[36] L. Mena, C. A. Monje, L. Nagua, J. Muñoz, and C. Balaguer, "Test bench for evaluation of a soft robotic link," *Frontiers Robot. AI*, vol. 7, p. 27, Mar. 2020. [Online]. Available: https://www.frontiersin.org/article/10.3389/frobt.2020.00027
[37] MPU. (2020). *Sensor MPU-6050 From Paradisetronic.com*. Accessed: Feb. 1, 2020. [Online]. Available: https://paradisetronic.com/de/mpu-6050-modul-3-achsen-gyroskop-3-achsen-accelerometer
[38] STM. (2020). *Control Board STM32F407*. Accessed: Feb. 1, 2020. [Online]. Available: https://www.st.com/en/evaluation-tools/stm32f4discovery.html
[39] A. F. Caballero, D. S. Copaci, Á. V. Peciña, D. B. Rojas, and L. M. Lorente, "Sistema avanzado de protipado Rápido para control en la Educación en Ingeniería para grupos multidisciplinares," *Revista Iberoamericana de Automática e Informática Ind. RIAI*, vol. 13, no. 3, pp. 350–362, Jul. 2016.
[40] Á. Villoslada, N. Escudero, F. Martín, A. Flores, C. Rivera, M. Collado, and L. Moreno, "Position control of a shape memory alloy actuator using a four-term bilinear PID controller," *Sens. Actuators A, Phys.*, vol. 236, pp. 257–272, Dec. 2015.
[41] A. Villoslada, A. Flores, D. Copaci, D. Blanco, and L. Moreno, "High-displacement flexible shape memory alloy actuator for soft wearable robots," *Robot. Auto. Syst.*, vol. 73, pp. 91–101, Nov. 2015.
[42] D. Copaci, L. Moreno, and D. Blanco, "Two-stage shape memory alloy identification based on the Hammerstein–Wiener model," *Frontiers Robot. AI*, vol. 6, p. 83, Sep. 2019. [Online]. Available: https://www.frontiersin.org/article/10.3389/frobt.2019.00083
[43] C.-H. Cheng, K.-H. Lin, and J.-L. Wang, "Co-contraction of cervical muscles during sagittal and coronal neck motions at different movement speeds," *Eur. J. Appl. Physiol.*, vol. 103, no. 6, p. 647, 2008.

DORIN COPACI received the degree in automatic control and systems engineering from the Politehnica University of Bucharest, Romania, in 2010, and the master's degree in robotics and automation and the Ph.D. degree in electrical, electronic, and automatic engineering from the Carlos III University of Madrid, Spain, in 2012 and 2017, respectively. Since 2010, he has been a Research Member with the Robotics Laboratory, Department of Systems Engineering and Automation, Carlos III University of Madrid.

JORGE MUÑOZ (Member, IEEE) received the M.Sc. degree in robotics and automation from the University Carlos III of Madrid, in 2011. He is currently pursuing the Ph.D. degree with the Robotics Laboratory Group, where he works with the humanoid robot TEO and the soft robotic neck from the HUMASOFT Project. He has been involved in projects like HANDLE (7th framework), the RoboticsLab Humanoid Robot TEO, and HumaSOFT. His research interest includes fractional and robust control for humanoids and soft robotics.

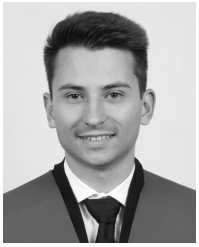

IGNACIO GONZÁLEZ received the degree in automation and industrial electronic engineering from the Carlos III University of Madrid, Spain, in 2019, where he is currently pursuing the master's degree in industrial engineering. His research interests include robotics, and control and industrial engineering.

CONCEPCIÓN A. MONJE (Member, IEEE) received the M.Sc. degree in electronics engineering from the Industrial Engineering School, University of Extremadura, Spain, in 2001, and the Ph.D. degree in industrial engineering from the University of Extremadura, in 2006. In September 2006, she joined the Department of Electronics and Electromechanical Engineering, University Carlos III of Madrid, as a Visiting Professor, where she is currently an Associate Professor. Her research interests include control theory and applications of fractional calculus to control systems and robotics. She has been a Principal Investigator in several EU and National research projects mainly related to these topics and has published over 100 technical articles on these fields.

LUIS MORENO (Member, IEEE) received the degree in automation and electronics engineering and the Ph.D. degree from the University Politécnica of Madrid, Spain, in 1984 and 1988, respectively. In 1994, he joined the Department of Systems Engineering and Automation, University Carlos III of Madrid, Madrid, Spain, where he has been involved in several mobile robotics projects. His research interests include mobile robotics, mobile manipulators, environment modeling, path planning, and mobile robot global localization problems.